Structural Engineering and Mechanics, *Vol. 76, No. 2 (2020) 153-162*
DOI: https://doi.org/10.12989/sem.2020.76.2.153

Effect of material mechanical differences on shear properties of contact zone composite samples: Experimental and numerical studies

Weiqi Wang[1,2], Yicheng Ye[1,2,3], Qihu Wang*[1,2,3], Xiaoyun Liu[1,2], Fan Yang[1] and Wenkan Tan[1]

[1]*School of Resources and Environmental Engineering, Wuhan University of Science and Technology, Wuhan 430-081, China*
[2]*Hubei Key Laboratory for Efficient Utilization and Agglomeration of Metallurgic Mineral Resources, Wuhan, 430-081, China*
[3]*Industrial Safety Engineering Technology Research Center of Hubei Province, Wuhan 430-081, China*

(Received February 7, 2020, Revised June 2, 2020, Accepted June 4, 2020)

Abstract. Aiming at the mechanical and structural characteristics of the contact zone composite rock, the shear tests and numerical studies were carried out. The effects of the differences in mechanical properties of different materials and the normal stress on shear properties of contact zone composite samples were analyzed from a macro-meso level. The results show that the composite samples have high shear strength, and the interface of different materials has strong adhesion. The differences in mechanical properties of materials weakens the shear strength and increase the shear brittleness of the sample, while normal stress will inhibit these effect. Under low/high normal stress, the sample show two failure modes, at the meso-damage level: elastic-shearing-frictional sliding and elastic-extrusion wear. This is mainly controlled by the contact and friction state of the material after damage. The secondary failure of undulating structure under normal-shear stress is the nature of extrusion wear, which is positively correlated to the normal stress and the degree of difference in mechanical properties of different materials. The increase of the mechanical difference of the sample will enhance the shear brittleness under lower normal stress and the shear interaction under higher normal stress.

Keywords: contact zone composite rock; difference in mechanical properties; contact interface; shear properties; failure mode

1. Introduction

There are a large number of composite structures composed of different materials in geotechnical engineering, such as composite rock composed of different types of rock (rock A-rock B), dam-dam foundation, shotcrete-surrounding rock and cemented paste backfill (CPB)-rock (Atapour and Moosavi 2013, Koupouli *et al.* 2016, Sarfarazi *et al.* 2016, Zhao *et al.* 2018). Different components and contact interfaces make the composite body susceptible to shear failure due to the effects of excavation and stress environment (Haeri *et al.* 2018, Müller *et al.* 2018, Tian *et al.* 2018, Liu *et al.* 2020). Therefore, the shear properties of composite bodies and contact interfaces are key issues for the stability of geotechnical structures.

A large number of studies on the shear behavior of concrete-rock and layered rock-rock have been carried out. The results show that the shear strength and failure characteristics of composites and interfaces are mainly affected by four factors: bond strength of interface (Moradian *et al.* 2012, Krounis *et al.* 2016, Pirzada *et al.* 2020), mechanical properties of component materials (Ghazvinian *et al.* 2010, Wu *et al.* 2018), normal stress (Tian *et al.* 2015) and interface morphology (Saiang *et al.* 2005, Champagne *et al.* 2013, Bista *et al.* 2020). Generally, the bond strength of the layered rock-rock interface is weak, and the shear characteristics are mainly affected by the normal stress, interface morphology, and differences in strength of different rocks (Li *et al.* 2015, Xia *et al.* 2018). Various factors mutually affect the shear strength, shear deformation (shear and normal) and failure surface morphology of composite bodies and interfaces (Ghazvinian *et al.* 2010, Moradian *et al.* 2010, Renaud *et al.* 2016, Shen *et al.* 2019). Affected by formation conditions and engineering background, the main controlling factors of shear properties of different composite bodies are different. Therefore, many studies have been conducted mainly on some factors of specific research objects (Andjelkovic *et al.* 2015, Krounis *et al.* 2015, Mouzannar *et al.* 2017, Haeri *et al.* 2019, Renaud *et al.* 2019, Lee *et al.* 2020).

The contact zone composite rock masses are formed by magmatic intrusion and metamorphism, and are widely found in rock engineering, especially in deep rock engineering, as shown in Fig. 1 (Ajalloeian *et al.* 2017, Cawood and Bond 2018, Antonellini *et al.* 2019). The engineering practice shows that when the tunnel or chamber passes through the contact zone, there are obvious stress concentration and differentiations in the rock masses near the contact interface (Yassaghi and Salari-Rad 2005, Feng *et al.* 2012). Convergence differences between different rock masses are obvious, and shear fractures appear near the interface of composite rock masses (Panda *et al.* 2014, Yang *et al.* 2019). Studies have shown that due to the difference in mechanical properties, uncoordinated deformation occurs in different rocks near the contact interface, which derives shear stress and causes shear failure at the interface (Xing *et*

*Corresponding author, Ph.D., Professor
E-mail: wangqihu@wust.edu.cn

http://www.techno-press.com/journals/sem&subpage=7
ISSN: 1225-4568 (Print), 1598-6217 (Online)

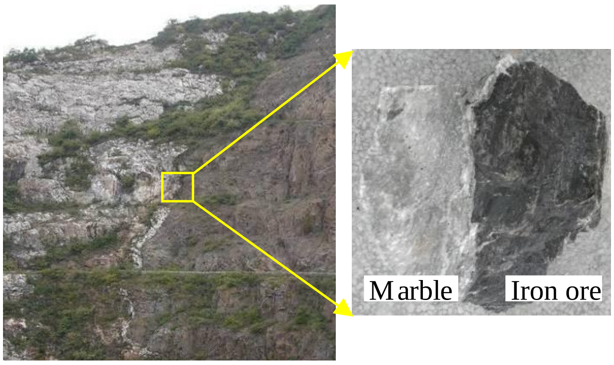

Fig. 1 Contact zone composite rock mass

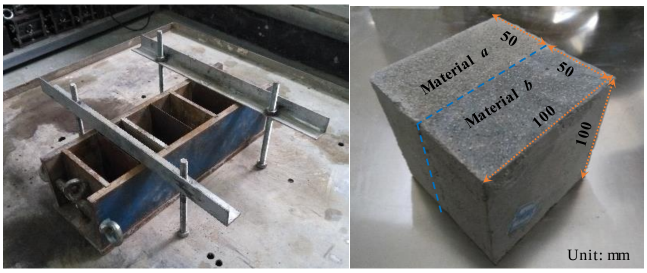

(a) Sample preparation (b) Composite sample

Fig. 2 Schematic diagram of sample preparation

al. 2019, Wang *et al*. 2020). The magnitude of derived shear stress is positively related to the degree of difference in mechanical properties of different rocks. These results show that the shear properties of rocks and interfaces have an important effect on the mechanical behavior of contact zone composite rocks.

The mechanical and structural characteristics of contact zone composite rocks are different from those of concrete-rock and layered composite rock due to the formation conditions and environment. The contact zone composite rocks have higher strength (Yassaghi and Salari-Rad 2005, Amann *et al*. 2011), and the uniaxial compressive strength ratio of different components is about 1~2, while the layered composite rock is about 1~8 (Feng *et al*. 2012, Douma *et al*. 2019). The interface of different component has stronger adhesion rather than weak adhesion or friction. At the same time, normal stress along the contact interface can reach up to 10 MPa in underground rock engineering, which is much higher than that of concrete-rock (0.15~0.8 MPa) (Moradian *et al*. 2010, Bahaadini *et al*. 2013).

Based on the research background stated above, it is necessary to carry out shear tests on contact zone composite rock to study the effects of normal stress (σ_n) and the differences in rock mechanical properties on the shear behavior of composite rocks and interfaces. Based on the experiment, a particle flow numerical model (PFC2D) was constructed to analyze the energy conversion and damage evolution characteristics of composite model during shearing, and to study the shear interaction from meso level. The test was carried out by preparing physically similar sample to overcome the disadvantages of sampling heterogeneity and the high testing cost of natural rock samples. Similar materials facilitate the preparation of composite samples with varying degrees of difference in mechanical properties.

2. Experimental methodologies

In order to ensure that the physical similar samples have good rock-like properties, P425 Portland cement, gypsum powder, river sand with particle diameters ranging from 0.9 to 1.2 mm and water were chosen as similar materials to make samples (Hu *et al*. 2019, Huang *et al*. 2019). The composite sample was designed to be a cube of 100 mm × 100 mm × 100 mm dimension. The ratios of five kinds of similar materials with different mechanical properties were determined by multiple adjustments and tests to simulate rocks with different mechanical properties. The ratios and mechanical parameters of five kinds of similar materials are listed in Table 1, where S represents the standard deviation of the data. Table 1 shows that the mechanical parameters of materials Nos. 1~5 have appropriate differences. The prism samples of 100 mm × 100 mm × 200 mm were prepared and the uniaxial compression tests were performed to obtain the elastic modulus of the materials in Table 1.

Two similar materials of uniform mixing were separately poured on both sides of specially designed mold of 100 mm × 100 mm × 100 mm dimension, and the mold was fixed on vibration table, as shown in Fig. 2(a). The mold frame was divided into two parts 50 mm in width. A thin vertical plate was inserted between two parts. The similar materials were shaken for one minute after filled, and then the plate was pulled out and shaken for another one minute to compact and bond the two similar materials. Figure 2(b) shows the prepared composite samples.

By combining two different materials, ten sets of composite samples with different degrees of difference in mechanical properties of the two materials were obtained. The composite samples were identified using *a*-*b*. Where *a* and *b* correspond to the material numbers in Table 1. The elastic modulus ratio of the two materials was defined as $\lambda=E_b/E_a$, which was used to quantified the degree of difference in mechanical properties of the two materials. The test selected five kinds of normal stress (σ_n) of 1 MPa, 2 MPa, 3 MPa, 4 MPa and 5 MPa. Three samples were sheared under each normal stress. The YZW-30A microcomputer controlled electronic rock shear machine was used to shear the sample at a rate of 0.002 mm/s.

3. Analysis of shear test results

3.1 Shear strength

The test results of the ten sets of composite samples are listed in Table 2, in which the cohesion and friction angles are obtained by fitting based on the Mohr-Coulomb criterion. Compared with the shear strength of a single material (Table 1), the shear strength of composite samples always lies between that of the strong material and the weak material under different normal stresses (σ_n) and degrees (λ) of difference in mechanical properties of materials. It shows that the contact interface of different materials of the

Table 1 Mechanical parameters of materials and corresponding material ratios

Sample number	Shear strength (S), τ (MPa)					Cohesion (S) (MPa)	Friction angle (S) (°)	Elastic modulus (GPa)	Cement/ gypsum	Sand/ plastic	Water/ cement
	$\sigma_n = 1$	$\sigma_n = 2$	$\sigma_n = 3$	$\sigma_n = 4$	$\sigma_n = 5$						
1	2.87 (0.03)	3.32 (0.07)	3.79 (0.06)	4.01 (0.13)	4.29 (0.15)	2.60 (0.10)	19.35 (1.78)	1.93	0.75	1.10	0.46
2	3.19 (0.06)	3.57 (0.05)	3.83 (0.01)	4.17 (0.02)	4.40 (0.42)	2.93 (0.04)	16.83 (0.75)	2.10	0.60	0.95	0.44
3	3.34 (0.08)	4.06 (0.04)	4.45 (0.05)	4.76 (0.06)	4.84 (0.01)	3.18 (0.22)	20.26 (3.85)	2.48	0.45	0.80	0.42
4	5.22 (0.02)	6.51 (0.15)	8.04 (0.21)	8.49 (0.01)	8.14 (0.34)	4.94 (0.74)	38.01 (12.58)	3.62	0.30	0.65	0.39
5	7.08 (0.21)	8.44 (0.13)	9.28 (0.26)	10.35 (0.38)	11.00 (0.25)	6.31 (0.22)	44.25 (3.72)	4.58	0.15	0.50	0.36

Table 2 Shear test results of composite samples

Sample number	Shear strength (S), τ (MPa)					Cohesion (S) (MPa)	Friction angle (S) (°)	Modulus ratio, λ
	$\sigma_n = 1$	$\sigma_n = 2$	$\sigma_n = 3$	$\sigma_n = 4$	$\sigma_n = 5$			
1-2	2.16 (0.12)	3.37 (0.23)	3.39 (0.39)	4.00 (0.07)	4.62 (0.17)	1.84 (0.30)	29.06 (5.20)	1.08
1-3	3.13 (0.15)	3.58 (0.46)	4.27 (0.23)	4.52 (0.21)	4.88 (0.01)	2.75 (0.13)	23.92 (2.30)	1.28
1-4	2.72 (0.20)	3.47 (0.02)	3.89 (0.11)	4.01 (0.09)	4.41 (0.27)	2.52 (0.21)	21.45 (3.56)	1.87
1-5	2.70 (0.06)	3.07 (0.08)	3.85 (0.06)	4.23 (0.16)	4.90 (0.20)	2.08 (0.12)	29.08 (2.01)	2.37
2-3	2.83 (0.03)	3.75 (0.17)	4.31 (0.04)	4.59 (0.04)	4.75 (0.04)	2.64 (0.30)	25.14 (5.10)	1.18
2-4	2.60 (0.30)	3.48 (0.05)	3.83 (0.03)	4.10 (0.04)	4.80 (0.21)	2.26 (0.20)	26.64 (3.41)	1.73
2-5	2.77 (0.13)	3.45 (0.05)	4.11 (0.08)	4.41 (0.01)	4.77 (0.21)	2.41 (0.17)	26.40 (2.98)	2.19
3-4	3.74 (0.03)	4.65 (0.05)	5.07 (0.17)	5.47 (0.11)	5.99 (0.34)	3.38 (0.18)	28.05 (3.07)	1.46
3-5	3.27 (0.08)	4.18 (0.19)	4.78 (0.25)	5.63 (0.06)	6.07 (0.03)	2.67 (0.14)	35.20 (2.47)	1.85
4-5	4.67 (0.22)	6.20 (0.17)	6.54 (0.10)	6.99 (0.24)	8.05 (0.15)	4.20 (0.38)	37.07 (6.46)	1.27

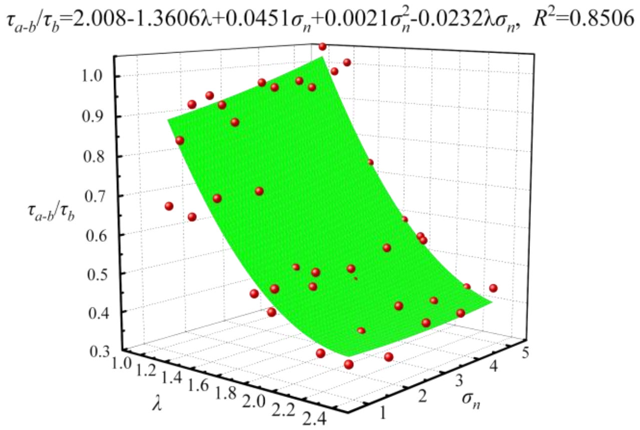

Fig. 3 Distribution of τ_{a-b}/τ_b with λ and σ_n

composite samples have high bond strength, which cannot be regarded as a general weak joint surface. The ratio of shear strength of composite sample (τ_{a-b}) to that of stronger material (τ_b) is defined as τ_{a-b}/τ_b. As shown in Fig. 3, σ_n and λ have obvious regular effects on τ_{a-b}/τ_b.

The difference in mechanical properties of materials shows a significant weakening effect on the shear strength of composite samples. As shown in Fig. 3, as the degree (λ) of difference increases, the shear strength of the composite sample gradually decreases compared to that of the stronger material, and gradually approaches that of the weaker material. Taking composite samples No. 1-3 (λ=1.28), No. 3-4 (λ=1.46) and No. 3-5 (λ=1.85) as examples, the ratios of τ_{a-b}/τ_b gradually decreases under 3MPa normal stress, which are 0.95, 0.69, and 0.51 respectively. It shows that the increase of λ will enhance its weakening effect on shear strength of composite samples.

The shear strength of the composite samples increases with the increase of the normal stress (σ_n), which accords with the general understanding (Koupouli *et al.* 2016, Tian *et al.* 2018). With the increase of normal stress, the shear strength of composite sample gradually increases compared to that of the stronger material (Fig. 3). Taking samples No. 3-5 as an example, the ratios of τ_{a-b}/τ_b are 0.46, 0.50, 0.51, 0.54 and 0.55, respectively, under 1~5 MPa normal stress. This shows that the normal stress can inhibit the weakening effect of the difference in material mechanical.

The test results show that the normal stress and the differences in mechanical properties of materials has opposite effects (increase/decrease) on the shear strength of composite samples. Increasing λ or decreasing σ_n will weaken the shear strength of the composite samples (Fig. 3). In the engineering environment, the normal stress is relatively fixed and uncontrollable. However, the mechanical properties of the surrounding rock can be adjusted by supporting means (Xing *et al.* 2019, Zhang *et al.* 2019). Therefore, adjusting the difference in mechanical properties of the rock mass is the main means to strengthen the shear strength of contact zone composite rock.

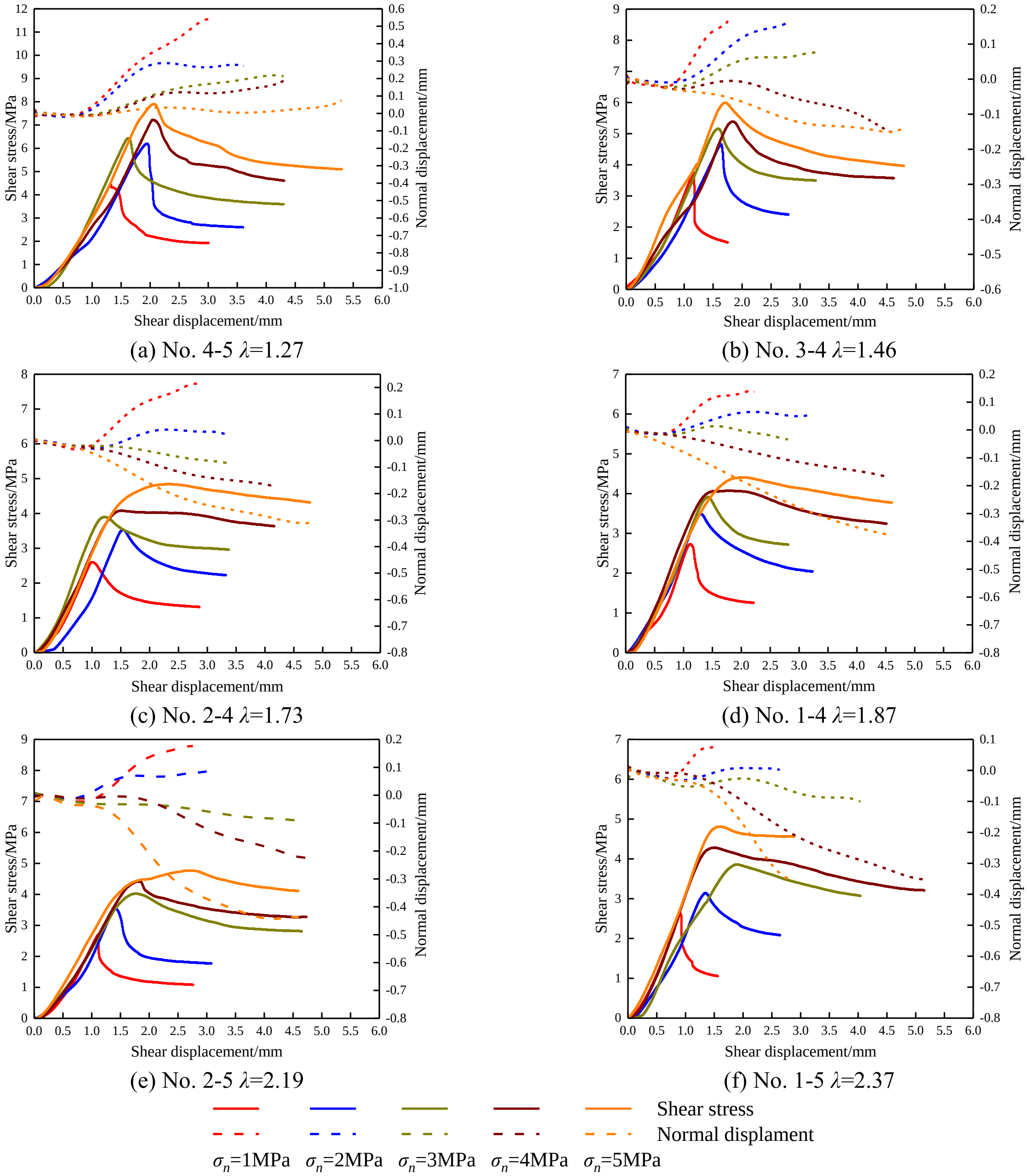

Fig. 4 Shear stress-shear displacement and normal displacement-shear displacement curves. Note that a positive slope of the normal displacement–shear displacement curves indicates dilation while a negative slope indicates compression

3.2 Shear deformation properties

Figure 4 shows the shear stress-shear displacement curves of the composite samples under different normal stresses. The results show that the shear stress increases linearly to the peak with the increase of shear displacement. However, after the peak shear stress, there are two type of shear behaviors under different normal stresses, which correspond to two typical curves.

• Under the lower normal stress, the shear stress drops sharply after the peak stress, showing brittle failure. Then, the shear stress slowly decreases to the residual strength.

• Under the higher normal stress, the shear stress gradually decreases in post-peak stage until the residual behavior.

This phenomenon was also observed in shear tests of concrete-rock. Analysis shows that this is due to the difference frictional force of the material after bond failure under different normal stresses (Saiang *et al*. 2005, Tian *et al*. 2015, Mouzannar *et al*. 2017). The comparison shows that the drop of shear stress is more obvious for the composite samples with larger λ, that is, the difference in mechanical properties of the two materials will increase the brittleness of the shear failure of the composite samples. For composite samples with components No. 1 or No. 2 material, under high normal stress, the shear peak is not

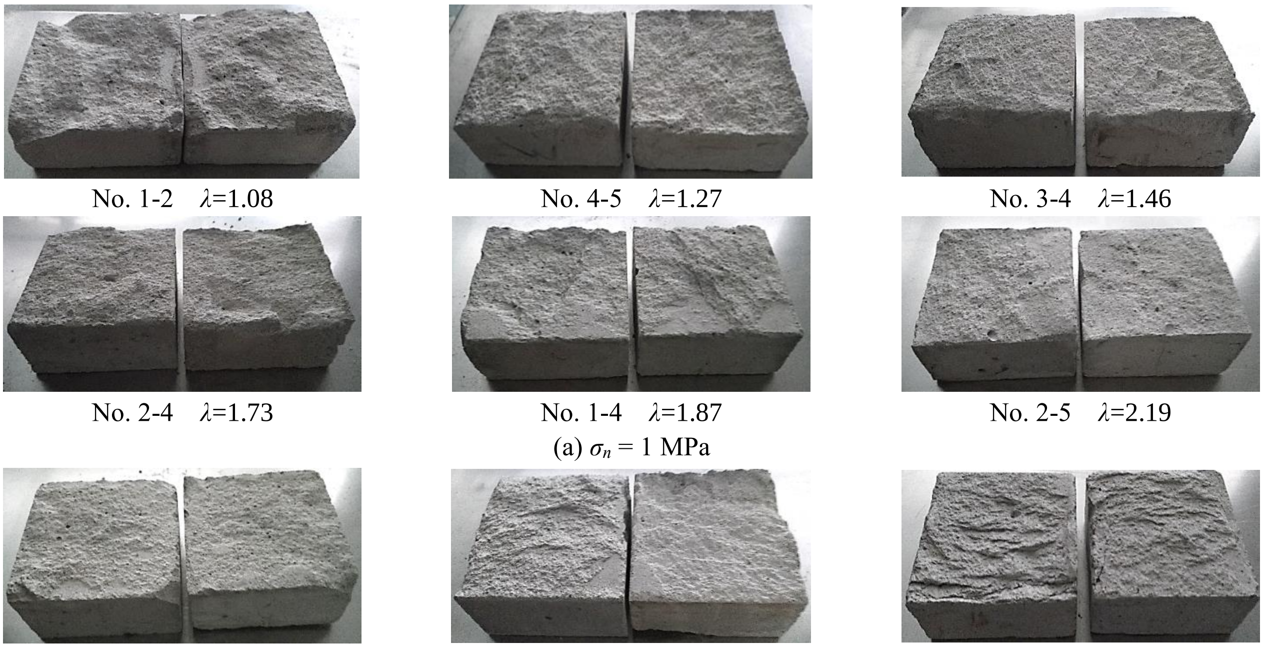

No. 1-2 λ=1.08 No. 4-5 λ=1.27 No. 3-4 λ=1.46

No. 2-4 λ=1.73 No. 1-4 λ=1.87 No. 2-5 λ=2.19

(a) σ_n = 1 MPa

σ_n=2MPa σ_n=3MPa σ_n=5MPa

(b) Sample No. 2-5

Fig. 5 Shear failure surface of composite sample

obvious and the curve after the peak declines slowly, showing a certain softening behavior (Figs. 4(c)-(f)). This indicates that the post-peak behavior of the sample is mainly controlled by the weak component material under high normal stress (Ghazvinian *et al*. 2010, Wu *et al*. 2018).

The dotted curves in Fig. 4 display the normal displacement of the composite sample during shearing. It was observed that the sample had a slight compression at the initial stage of shear. In the subsequent shearing process, the sample exhibited dilation under low normal stress. As the normal stress increased, the dilation gradually weakened and eventually turned to compression. By comparison, the normal stress required for the sample with a larger λ to change from dilation to compression is lower. For example, samples No. 2-4 (λ=1.73) and No. 3-4 (λ=1.46), show compression under normal stress of 3 MPa and 4 MPa, respectively (Figs. 4(b)-(c)). Under the same normal stress, samples with larger λ produce smaller dilation or greater compression. These results show that the stronger material will damage the weaker material in the shear process, and there is extrusion wear, which is positively correlated with the degree of differences in material mechanical. This is the main form of weak material controlling the shear behavior of composite sample under high normal stress.

3.3 Characteristics of shear failure surface

The forms of the shear failure of the composite samples were observed. As shown in Fig. 5, the normal stress and the differences in mechanical properties of the materials have a significant effect on the location and morphology of the shear failure surface of the composite samples.

The failure surface of composite sample always formed at the weak material side near the contact interface, and the weak material is locally bonded to the strong material side. Comparing the samples with different mechanical differences in materials (Fig. 5(a)), it is found that with the increase of λ, the weak materials bonded on the strong material side becomes thinner, and the failure surface approaches the contact interface gradually. The analysis shows that the bond strength of the contact interface decreases with the increase of the mechanical difference, which makes the shear failure easier to form near the interface rather than in the weak material. Zhao *et al*. (2018) found similar results in the shear tests of foam concrete-rock.

The shear failure surface morphology of the composite samples is affected by the normal stress and the difference in mechanical properties of the materials. Under low normal stress (Fig. 5(a)), the surface morphology of the sample with small difference in material mechanical has many crests with large undulation. With the increase of the difference in material mechanical, the surface tends to flatten, showing a brittle shear failure. However, for composite samples with larger λ, the increase of normal stress will aggravate the undulation of shear failure surface. Taking sample No. 2-5 as an example (Fig. 5(b)), as the normal stress increases, the failure surface gradually changes from flat to many smaller crests. These results indicate that the influence of normal stress on the morphology of the failure surface is affected by the mechanical differences of the materials, which is different from the general conclusion that increasing normal stress will reduce the undulation of the failure surface (Ghazvinian *et al*. 2010, Li *et al*. 2015). Analysis shows that this can be attributed to two reasons: first, the difference in mechanical properties of the material will increase the brittleness of shear failure, and second, the extrusion wear will occur more easily under high normal stress.

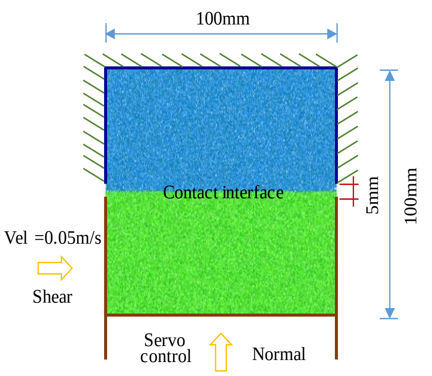

Fig. 6 Shear test model of composite sample

Table 3 Mesoscopic parameters of the numerical model

Minimum radius (mm)	Radius ratio	Density (kg/m^3)	Friction coefficient	Radius multiplier	Proximity (mm)
0.35	1.44	3600	1.0	1.5	$1.8e^{-5}$

Table 4 Mesoscopic parameters of three types of numerical

Mesoscopic parameters		Sample number 2	4	5
Particle				
E	Effective modulus (GPa)	0.40	0.68	0.57
k_n / k_s	Stiffness ratio	2.70	3.10	2.85
Parallel bond				
$\bar{E}$	Effective modulus (GPa)	0.40	0.68	0.57
$\bar{k}_n / \bar{k}_s$	Stiffness ratio	2.70	3.10	2.85
$\bar{\sigma}_t$	Tensile strength (MPa)	3.60 ± 0.72	8.20 ± 1.64	6.13 ± 1.23
$\bar{\sigma}_c$	Cohesion (MPa)	4.02 ± 0.80	8.83 ± 1.77	6.08 ± 1.22

4. Numerical simulation of shear failure

4.1 Model construction and calibration

The shear failures of composite samples No. 2-5 and No. 4-5 under normal stress of 1 MPa and 3 MPa were simulated, respectively, and the effects of the difference in mechanical properties of the materials and the normal stress on the sample were studied from a meso level.

As shown in Fig. 6, the composite model is 100 mm × 100 mm and is divided into two parts 50 mm in height along the normal direction, representing the two materials that constitute the composite sample. Control the activation direction of the wall in the model, so that the two material elements at the contact interface contact freely within the range of 1 times the minimum particle radius in the normal direction to form a realistic contact interface. The numerical model used the parallel bonding model, and the mesoscopic parameters of the interface are the same as those of the stronger material. The numerical model of a single material is different from the composite model only in the component of the material.

Table 5 Reduction factors of mesoscopic parameters

Model number	Normal stress (MPa)	k_E	k_r	k_t	k_c
2-5	1	0.73	1.47	0.60	0.64
	3	0.60	0.76	1.08	0.63
4-5	1	0.90	1.52	0.68	0.66
	3	0.96	0.95	1.13	0.76

There are many mesoscopic parameters in the numerical model, and there is no clear relationship between the mesoscopic parameters and the macro response. As listed in Table 3, the parameters with a weaker influence on the model were set in advance. Subsequently, the orthogonal design method (Khazaei *et al*. 2015, Wang *et al*. 2020), which involves changing one parameter while keeping other parameters constant, was used and a series of tests were conducted based on the test results of the single material sample in Table 1. Finally, the mesoscopic parameters of the three types of single models were determined and listed in Table 4.

The calibration of the meso-parameters of the composite model was achieved by reducing the mesoscopic parameters of the single material models and assigning them to different component materials of the composite model. The reduction is mainly due to the size effect between the composite model material and the single model material, and the interaction between the different materials. The modulus (E, $\bar{E}$, k_n/k_s, $\bar{k}_n / \bar{k}_s$) and strength ($\bar{\sigma}_t$, $\bar{\sigma}_c$) parameters of the two component materials are respectively multiplied by the same factor to achieve the reduction. The reduction factors of elastic modulus, stiffness ratio, tensile strength and cohesion were defined as k_E, k_r, k_t and k_c, respectively. Based on the test results, after a series of tests, the reduction factors corresponding to the composite models No. 2-5 and No. 4-5 under normal stresses of 1 MPa and 3 MPa were determined, respectively, as listed in Table 5.

4.2 Shear damage evolution model

The energy conversion and crack development characteristics of composite samples under different normal stress were observed, as shown in Fig. 7. The results show that under different normal stresses, the shear damage evolution of the composite model can be divided into two typical modes, corresponding to two typical shear stress-shear displacement curves in Section 3.2.

Mode 1: Elastic-shearing-frictional sliding

As shown in Figs. 7(a)-(b), under low normal stress, the model is in the elastic state at pre-peak stage. The strain energy and bond energy of the model increases with the increase of the boundary energy, and the frictional energy is lowered. When the shear stress reaches the peak value, the shearing failure occurs. The strain energy and bond energy decrease sharply, and the frictional energy increases rapidly, with the rapid growth of tensile cracks. After shearing, the materials on both sides of the failure surface frictional sliding, the strain energy and bond energy gradually

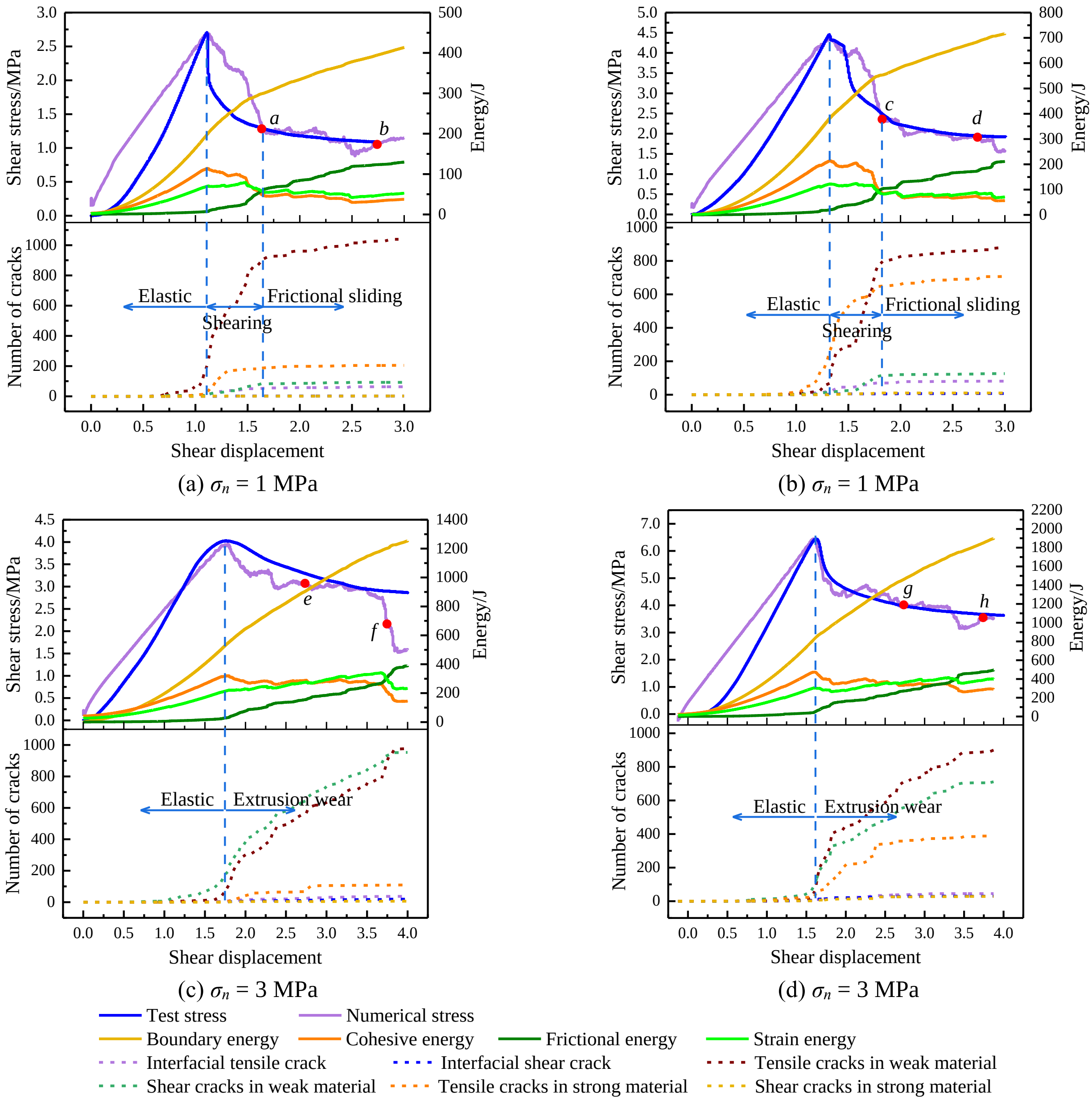

Fig. 7 Shear damage evolution of the composite model under normal stresses of 1 MPa and 3 MPa. (a), (c) Model No. 2-5, λ = 2.19 and (b), (d) model No. 4-5, λ = 1.27

decrease, and the frictional energy slowly increases, with a small number of tensile cracks.

Mode 2: Elastic-extrusion wear

As shown in Figs. 7(c)-(d), under high normal stress, the pre-peak stage of the model is similar to the elastic phase of model 1. The extrusion wear of the model occurred at post-peak stage. The strain energy and frictional energy of the model increase slowly, while the bond energy decreases slowly. Tensile-shear cracks generates in the model and increase continuously. There were several small fluctuations in the increase of the bond energy and number of cracks, indicating that there were many local shearing failures.

The contact and friction states of the model elements after bond failure under different normal stresses are the main factors that form the two evolution modes. The analysis shows that under low normal stress, the contact force of the particles disappears or changes into sliding friction force immediately after bond failure, the bond failure expands rapidly, shear stress decreases greatly, and it appears as a brittle failure on macro (mode 1). Under high normal stress, the particles remain in close contact after the bond failure, there is a large frictional force, and the bond failure gradually, resulting in a gradual decrease in shear stress, and no brittle failure characteristics on macro (mode 2). In addition, the linear increase of frictional energy under high normal stress indicates that the magnitude of the frictional force is relatively stable, which is different from the conclusion that the frictional force increases gradually during the shearing of concrete-rock (Saiang *et al*. 2005, Tian *et al*. 2015). These results can explain the formation mechanism of two typical shear stress-shear displacement curves at meso level.

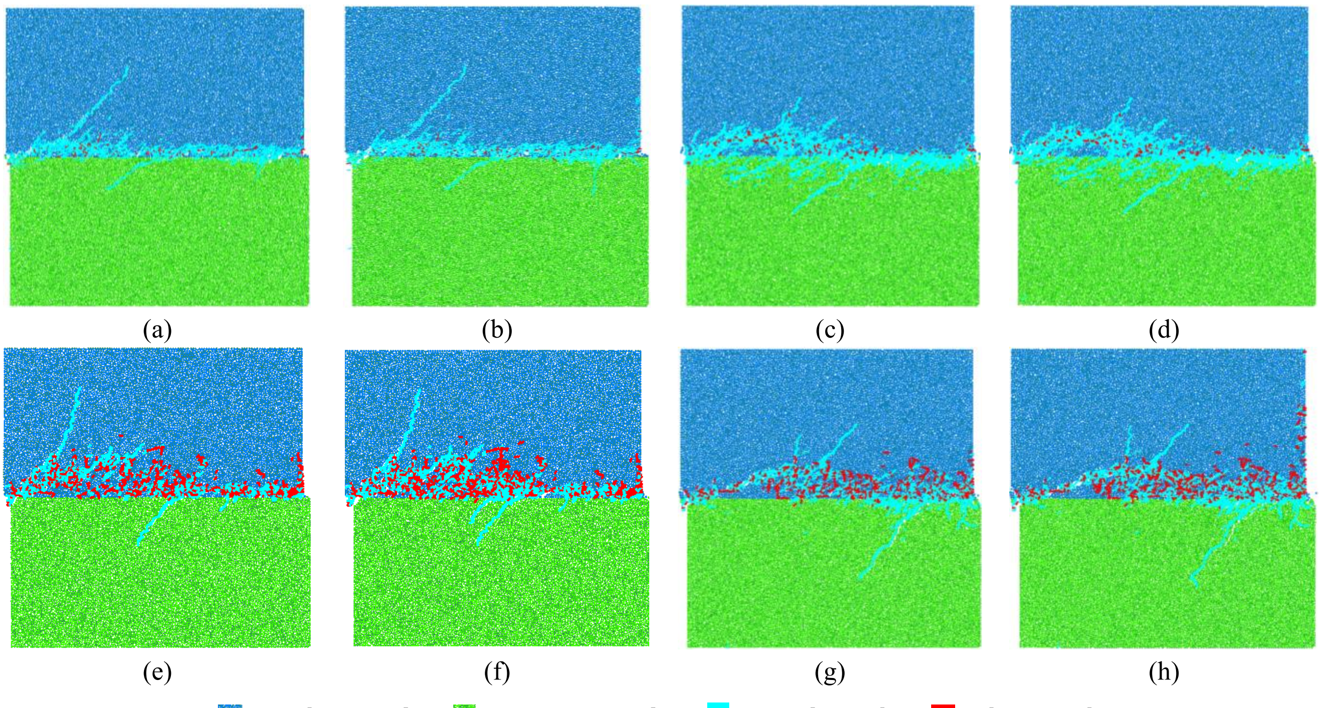

Fig. 8 The crack distribution of the composite model under different shear states, and the positions of the state points $a \sim h$ are shown in Fig. 7

4.3 Shear interaction of composite model

The distribution and development of cracks during the shearing process of the composite model were observed. Figure 8 shows the crack distribution of the composite model under different shear states, in which points *a* and *c* represent the shearing position, points *b*, *d*, *e* and *g* represent the shear displacement of 2.75 mm, and points *f* and *h* represent the shear displacement of 3.75 mm, as shown in Fig. 7.

The analysis shows that extrusion wear is the main form of shear interaction of the composite model under high normal stress. After the model is sheared under low normal stress, the materials on both sides of the failure surface slides along the surface, and the number and distribution of cracks change a little (Figs. 8(a)-(d)). Under high normal stress, the materials on both sides of the failure surface continued to be damaged in post-peak stage, and the cracks in the weak material near the failure surface continued to expand (Figs. 8(e)-(h)). Therefore, the nature of extrusion wear in mode 2 is the secondary failure of the undulating structure formed at the pre-peak stage of the model under high normal stress.

Analysis of the types and locations of cracks revealed that compared with low normal stresses, more cracks were generated in the weak material under high normal stress, more shear cracks than tensile cracks, and fewer cracks in the strong material. The results show that with the increase of normal stress, the failure type of the weak material changes from tensile to tension-shear, which aggravates the extrusion wear of the model.

The differences in mechanical properties of the materials have a significant effect on the shear brittleness and interaction of the composite model. Under low normal stress, the failure surface of model No. 2-5 (λ=2.19) is flatter than that of model No. 4-5 (λ=1.27), and the crack distribution is more concentrated (Figs. 8(a)-(d)). Under high normal stress, the failure of weak materials in model No. 2-5 is more serious, the cracks distribution is wider, and the shear cracks are more (Figs. 8(e)-(h)). Therefore, the increase of the mechanical difference of the sample will enhance the shear brittleness under lower normal stress and the shear interaction under higher normal stress. This is consistent with the test results in Section 3.3.

5. Conclusions

Based on the analysis of the test and numerical simulation, some conclusions have been made as follows:

- The differences in mechanical properties of the materials and the normal stress have obvious regular effects on the shear strength of contact zone composite samples. The shear strength of composite sample lies between that of the two component materials, and the interface between different materials has a high bond strength and cannot be regarded as a weak surface. The differences in mechanical properties of the materials weaken the shear strength of the composite sample, and the normal stress will inhibit the weakening.
- Due to the difference in brittleness, the composite samples exhibit two typical shear deformation modes under different normal stresses, corresponding to two meso-damage evolution modes: elastic-shearing-frictional sliding and elastic-extrusion wear. Under low normal stress, the

contact of material disappears or becomes sliding friction immediately after bond failure, but under high normal stress, the material still maintains close contact after bond failure, and there is larger frictional force, and the bond failure gradually.

- There is extrusion wear between the materials of the composite model under high normal stress, which is positively correlated with normal stress and the degree of differences in mechanical properties of the materials. The nature of extrusion wear is the secondary failure of the failure structure under normal-shear stress. Increasing the normal stress will cause the change of failure type from tensile to tensile-shear. Under high normal stress, the extent and range of extrusion wear will increase as the degree of difference in mechanical properties of materials increases.
- The position of the shear failure surface of the composite sample gradually approaches the interface with the increase of the difference in mechanical properties of the materials. Increasing the normal stress will aggravate the undulation of the failure surface, and the influence of the difference in materials on failure surface is related to normal stress. This is attributed to the fact that the difference in mechanical properties of the material increases the brittleness of shear failure under low normal stress. However, the material is more susceptible to extrusion wear under high normal stress.

Acknowledgments

The authors acknowledge the financial support from the National Natural Science Foundation of China (Nos. 51704213, 51804224 and 51574183), the Special Project of Central Government for Local Science and Technology Development of Hubei Province (2019ZYYD060) and the Open Fund of Hubei Key Laboratory for Efficient Utilization and Agglomeration of Metallurgic Mineral Resources (No. 2019zy002).

References

Ajalloeian, R., Moghaddam, B. and Azimian, A. (2017), “Prediction of rock mass squeezing of T4 tunnel in Iran”, *Geotech. Geol. Eng.*, **35**(2), 747-763. https://doi.org/10.1007/S10706-016-0139-Y.

Amann, F., Button, E.A., Evans, K.F., Gischig, V.S. and Blümel, M. (2011), “Experimental study of the brittle behavior of clay shale in rapid unconfined compression”, *Rock Mech. Rock Eng.*, **44**(4), 415-430. https://doi.org/10.1007/s00603-011-0156-3.

Andjelkovic, V., Pavlovic, N., Lazarevic, Z. and Nedovic, V. (2015), “Modelling of shear characteristics at the concrete–rock mass interface”, *Int. J. Rock Mech. Min. Sci.*, **76**, 222-236. http://dx.doi.org/10.1016/j.ijrmms.2015.03.024.

Antonellini, M., Nannoni, A., Vigna, B. and Waele, J.D. (2019), “Structural control on karst water circulation and speleogenesis in alithological contact zone: The Bossea cave system (Western Alps, Italy)”, *Geomorphology.*, **345**, 1-21. https://doi.org/10.1016/j.geomorph.2019.07.019.

Atapour, H. and Moosavi, M. (2013), “Some Effects of Shearing Velocity on the Shear Stress-Deformation Behaviour of Hard–Soft Artificial Material Interfaces”, *Geotech. Geol. Eng.*, **31**(5), 1603-1615. http://dx.doi.org/10.1007/s10706-013-9687-6.

Bahaadini, M., Sharrock, G. and Hebblewhite, B. (2013), “Numerical direct shear tests to model the shear behaviour of rock joints”, *Comput. Geotech.*, **51**, 101-115. https://doi.org/10.1016/j.compgeo.2013.02.003.

Bista, D., Sas, G., Johansson, F. and Lia, L. (2020), “Influence of location of large-scale asperity on shear strength of concrete-rock interface under eccentric load”, *J. Rock Mech. Geotech. Eng.*, https://doi.org/10.1016/j.jrmge.2020.01.001.

Cawood, A.J. and Bond, C.E. (2018), “3D mechanical stratigraphy of a deformed multi-layer: Linking sedimentary architecture and strain partitioning”, *J. Struct. Geol.*, **106**, 54-69. https://doi.org/10.1016/j.jsg.2017.11.011.

Champagne, K., Rivard, P. and Quirion, M. (2013), “Paramètres de résistance au cisaillement associés aux discontinuités des barrages en béton du Québec”, *Annual Conference of Canadian Dam Association*, Montréal, Québec, Canada.

Douma, L.A.N.R., Regelink, J.A., Bertotti, G., Boersma, Q.D. and Barnhoorn, A. (2019), “The mechanical contrast between layers controls fracture containment in layered rocks”, *J. Struct. Geolo.*, **127**, 1-11. https://doi.org/10.1016/j.jsg.2019.06.015.

Feng, W.K., Huang, R.Q. and Li, T.B. (2012), “Deformation analysis of a soft–hard rock contact zone surrounding a tunnel”, *Tunn. Undergr. Sp. Technol.*, **32**, 190-197. http://dx.doi.org/10.1016/j.tust.2012.06.011.

Ghazvinian, A.H., Taghichian, A., Hashemi, M. and Mar’ashi, S.A. (2010), “The shear behavior of bedding planes of weakness between two different rock types with high strength difference”, *Rock Mech. Rock Eng.*, **43**(1), 69-87. http://dx.doi.org/10.1007/s00603-009-0030-8.

Haeri, H., Sarfarazi, V. and Zhu, Z. (2018), “Numerical simulation of the effect of bedding layer geometrical properties on the punch shear test using PFC3D”, *Struct. Eng. Mech.*, **68**(4), 507-517. https://doi.org/10.12989/SEM.2018.68.4.507.

Haeri, H., Sarfarazi, V., Zhu, Z., Hokmabadi, N. N., Moshrefifar, M. and Hedayat, A. (2019), “Shear behavior of non-persistent joints in concrete and gypsum specimens using combined experimental and numerical approaches”, *Struct. Eng. Mech.*, **69**(2), 221-230. https://doi.org/10.12989/SEM.2019.69.2.221.

Hu, B., Yang, S.Q., Xu, P. and Cheng, J.L. (2019), “Cyclic loading–unloading creep behavior of composite layered specimens”, *Acta Geophys.*, **67**(2), 449-464. https://doi.org/10.1007/s11600-019-00261-x.

Huang, C.C., Yang, W.D., Duan, K., Fang L.D., Wang L. and Bo, C.J. (2019), “Mechanical behaviors of the brittle rock-like specimens with multi-non-persistent joints under uniaxial compression”, *Constr. Build. Mater.*, **220**, 426-443. https://doi.org/10.1016/j.conbuildmat.2019.05.159.

Khazaei, C., Hazzard, J. and Chalaturnyk, R. (2015), “Damage quantification of intact rocks using acoustic emission energies recorded during uniaxial compression test and discrete element modeling”, *Comput. Geotech.*, **67**, 94-102. https://doi.org/10.1016/j.compgeo.2015.02.012.

Koupouli, N.J.F., Belem, T., Rivard, P. and Effenguet, H. (2016), “Direct shear tests on cemented paste backfill-rock wall and cemented paste backfill-backfill interfaces”, *J. Rock Mech. Geotech. Eng.*, **8**(4), 472-479. http://dx.doi.org/10.1016/j.jrmge.2016.02.001.

Krounis, A., Johansson, F. and Larsson, S. (2015), “Effects of spatial variation in cohesion over the concrete-rock interface on dam sliding stability”, *J. Rock Mech. Geotech. Eng.*, **7**(6), 659-667. http://dx.doi.org/10.1016/j.jrmge.2015.08.005.

Krounis, A., Johansson, F. and Larsson, S. (2016), “Shear strength of partially bonded concrete–rock interfaces for application in dam stability analyses”, *Rock Mech. Rock Eng.*, **49**(7), 2711-2722. https://doi.org/10.1007/s00603-016-0962-8.

Li, W.F., Bai, J.B., Cheng, J.Y., Peng, S. and Liu, H.L. (2015), "Determination of coal–rock interface strength by laboratory direct shear tests under constant normal load", *Int. J. Rock Mech. Min. Sci.*, **77**, 60-67. http://dx.doi.org/10.1016/j.ijrmms.2015.03.033.

Lee, J.S., Han, W., Kim, S.Y. and Byun, Y.H. (2020), "Shear strength and interface friction characteristics of expandable foam grout", *Constr. Build. Mater.*, **249**, 1-10. https://doi.org/10.1016/j.conbuildmat.2020.118719.

Moradian, Z.A., Ballivy, G. and Rivard, P. (2012), "Application of acoustic emission for monitoring shear behavior of bonded concrete–rock joints under direct shear test", *Can. J. Civ. Eng.*, **39**(8), 887-896. https://doi.org/10.1139/L2012-073.

Moradian, Z.A., Ballivy, G., Rivard, P., Gravel, C. and Rousseau, B. (2010), "Evaluating damage during shear tests of rock joints using acoustic emissions", *Int. J. Rock Mech. Min. Sci.*, **47**(4), 590-598. https://doi.org/10.1016/j.ijrmms.2010.01.004.

Mouzannar, H., Bost, M., Leroux, M. and Virely, D. (2017), "Experimental study of the shear strength of bonded concrete–rock interfaces: surface morphology and scale effect", *Rock Mech. Rock Eng.*, **50**(10), 2601-2625. https://doi.org/10.1007/s00603-017-1259-2.

Müller, C., Frühwirt, T., Haase, D., Schlegel, R. and Konietzky, Heinz. (2018), "Modeling deformation and damage of rock salt using the discrete element method", *Int. J. Rock Mech. Min. Sci.*, **103**, 230-241. https://doi.org/10.1016/j.ijrmms.2018.01.022.

Panda, M.K., Mohanty, S., Pingua, B.M.P. and Mishra, A.K. (2014), "Engineering geological and geotechnical investigations along the head race tunnel in Teesta Stage-III hydroelectric project, India", *Eng. Geol.*, **181**, 297-308. http://dx.doi.org/10.1016/j.enggeo.2014.08.022.

Pirzada, M.A., Roshan, H., Sun, H., Oh, J., Andersen, M.S., Hedayat, A. and Bahaaddini, M. (2020), "Effect of contact surface area on frictional behaviour of dry and saturated rock joints", *J. Struct. Geol.*, **135**, 1-12. https://doi.org/10.1016/j.jsg.2020.104044.

Renaud, S., Bouaanani, N. and Miquel, B. (2016), "Critical appraisal of common simplified assumptions in seismic stability analyses of gravity dams", *J. Perform. Constr. Facil.*, **30**(5), 04016017. http://dx.doi.org/10.1061/(ASCE)CF.1943-5509.0000843.

Renaud, S., Saichi, T., Bouaanani, N., Miquel, B., Quirion, M. and Rivard, P. (2019), "Roughness effects on the shear strength of concrete and rock joints in dams based on experimental data", *Rock Mech. Rock Eng.*, **52**(10), 3867-3888. https://doi.org/10.1007/s00603-019-01803-x.

Saiang, D., Malmgren, L. and Nordlund, E. (2005), "Laboratory tests on shotcrete-rock joints in direct shear, tension and compression", *Rock Mech. Rock Eng.*, **38**(4), 275-297. http://dx.doi.org/10.1007/s00603-005-0055-6.

Sarfarazi, V., Haeri, H. and Khaloo, A. (2016), "The effect of non-persistent joints on sliding direction of rock slopes", *Comput. Concr.*, **17**(6), 723-737. https://doi.org/10.12989/CAC.2016.17.6.723.

Shen, Y.J., Wang, Y.Z., Yang, Y., Sun, Q., Luo, T. and Zhang, H. (2019), "Influence of surface roughness and hydrophilicity on bonding strength of concrete-rock interface", *Constr. Build. Mater.*, **213**, 156-166. https://doi.org/10.1016/j.conbuildmat.2019.04.078.

Tian, H.M., Chen, W.Z., Yang, D.S. and Yang, J.P. (2015), "Experimental and numerical analysis of the shear behaviour of cemented concrete–rock joints", *Rock Mech. Rock Eng.*, **48**(1), 213-222. https://doi.org/0.1007/s00603-014-0560-6.

Tian, Y.C., Liu, Q.S., Ma, H., Liu, Q. and Deng, P.H. (2018), "New peak shear strength model for cement filled rock joints", *Eng. Geol.*, **233**, 269-280. https://doi.org/10.1016/j.enggeo.2017.12.021.

Wang, W.Q., Ye, Y.C., Wang, Q.H., Liu, X.Y., Yuan, Z.H. and Li, P.C. (2020), "Effects of differences in mechanical parameters of media on mechanical properties and failure form of composite samples", *KSCE. J. Civ. Eng.*, **24**(2), 424-434. https://doi.org/10.1007/s12205-020-1021-2.

Wang, W.Q., Ye, Y.C., Wang, Q.H., Luo, B.Y., Wang, J. and Liu, Y. (2020), "Interaction and mechanical effect of materials interface of contact zone composite samples: Uniaxial compression experimental and numerical studies", *Geomech. Eng.*, **21**(6), 571-582. https://doi.org/10.12989/gae.2020.21.6.571.

Wu, Q., Xu, Y.J., Tang, H.M., Fang, K., Jiang, Y.F., Liu, C.Y., Wang, L.Q., Wang, X.H. and Kang, J.T. (2018), "Investigation on the shear properties of discontinuities at the interface between different rock types in the Badong formation, China", *Eng. Geol.*, **245**, 280-291. https://doi.org/10.1016/j.enggeo.2018.09.002.

Xia, L., Zeng, Y.W., Luo, R. and Liu, W. (2018), "Influence of bedding planes on the mechanical characteristics and fracture pattern of transversely isotropic rocks in direct shear tests", *Shock Vib.*, **2018**, 1-14. https://doi.org/10.1155/2018/6479031.

Xing, Y., Kulatilake, P.H.S.W. and Sandbak, L.A. (2019), "Stability Assessment and Support Design for Underground Tunnels Located in Complex Geologies and Subjected to Engineering Activities: Case Study", *Int. J. Geomech.*, **19**(5), 1-9. https://doi.org/10.1061/(ASCE)GM.1943-5622.0001402.

Yang, S.Q., Tao, Y., Xu, P. and Chen, M. (2019), "Large-scale model experiment and numerical simulation on convergence deformation of tunnel excavating in composite strata", *Tunn. Undergr. Sp. Technol.*, **94**, 1-18. https://doi.org/10.1016/j.tust.2019.103133.

Yassaghi, A. and Salari-Rad, H. (2005), "Squeezing rock conditions at an igneous contact zone in the Taloun tunnels, Tehran-Shomal freeway, Iran: a case study", *Int. J. Rock Mech. Min. Sci.*, **42**(1), 95-108. https://doi.org/10.1016/j.ijrmms.2004.07.002.

Liu, Y., Ye, Y.C., Wang, Q.H. and Wang, W.Q. (2020), "Experimental Research on Shear Failure Monitoring of Composite Rocks Using Piezoelectric Active Sensing Approach", *Sensors.*, **20**(5), 1-17. http://dx.doi.org/10.3390/s20051376.

Zhang, Q.Y., Ren, M.Y., Duan, K., Wang, W.S., Gao, Q., Lin, H.X., Xiang, W. and Jiao, Y.Y. (2019), "Geo-mechanical model test on the collaborative bearing effect of rock-support system for deep tunnel in complicated rock strata", *Tunn. Undergr. Sp. Technol.*, **91**, 103001. https://doi.org/10.1016/j.tust.2019.103001.

Zhao, W.S., Chen, W.Z. and Zhao, K. (2018), "Laboratory test on foamed concrete-rock joints in direct shear", *Constr. Build. Mater.*, **173**, 69-80. https://doi.org/10.1016/j.conbuildmat.2018.04.006.

CC